ARMY RESEARCH LABORATORY

Thermal Analysis for a 37-mm Gun Chamber With Ceramic Nozzles

by Xiaogang Huang, James Garner, and Paul Conroy

ARL-MR-624 **September 2005**

NOTICES

Disclaimers

The findings in this report are not to be construed as an official Department of the Army position unless so designated by other authorized documents.

Citation of manufacturer's or trade names does not constitute an official endorsement or approval of the use thereof.

Destroy this report when it is no longer needed. Do not return it to the originator.

Army Research Laboratory
Aberdeen Proving Ground, MD 21005-5066

ARL-MR-624 **September 2005**

Thermal Analysis for a 37-mm Gun Chamber With Ceramic Nozzles

Xiaogang Huang, James Garner, and Paul Conroy
Weapons and Materials Research Directorate, ARL

REPORT DOCUMENTATION PAGE	Form Approved OMB No. 0704-0188

1. REPORT DATE *(DD-MM-YYYY)*	2. REPORT TYPE	3. DATES COVERED (From - To)
September 2005	Final	2004–2005

4. TITLE AND SUBTITLE
Thermal Analysis for a 37-mm Gun Chamber With Ceramic Nozzles

5a. CONTRACT NUMBER

5b. GRANT NUMBER

5c. PROGRAM ELEMENT NUMBER

6. AUTHOR(S)
Xiaogang Huang, James Garner, and Paul Conroy

5d. PROJECT NUMBER
622618.H8011

5e. TASK NUMBER

5f. WORK UNIT NUMBER

7. PERFORMING ORGANIZATION NAME(S) AND ADDRESS(ES)
U.S. Army Research Laboratory
ATTN: AMSRD-ARL-WM-BC
Aberdeen Proving Ground, MD 21005-5066

8. PERFORMING ORGANIZATION REPORT NUMBER
ARL-MR-624

9. SPONSORING/MONITORING AGENCY NAME(S) AND ADDRESS(ES)

10. SPONSOR/MONITOR'S ACRONYM(S)

11. SPONSOR/MONITOR'S REPORT NUMBER(S)

12. DISTRIBUTION/AVAILABILITY STATEMENT
Approved for public release; distribution is unlimited.

13. SUPPLEMENTARY NOTES

14. ABSTRACT

The 37-mm interior ballistics chamber is primarily a test bed to evaluate new propellant properties and their effects on gun systems. Experiments were conducted examining the properties of various ceramics under realistic interior ballistic loadings. The thermal response during the launch will cause stresses due to the large temperature gradient and coefficient of thermal expansion mismatch between the ceramic nozzle and steel gun chamber. In the first step of the investigation, it is essential to determine the thermal stress created. This report details the finite-element model used to predict the thermal response of the chamber and selected ceramic nozzle samples to better understand the sources or modes of failure observed in chamber firings. These results are essential in guiding the selection of nozzle materials and research into the use of ceramics in a gun chamber.

15. SUBJECT TERMS
thermal conductive, ceramic nozzle, ABAQUS code, thermal erosion

16. SECURITY CLASSIFICATION OF:			17. LIMITATION OF ABSTRACT	18. NUMBER OF PAGES	19a. NAME OF RESPONSIBLE PERSON
a. REPORT	b. ABSTRACT	c. THIS PAGE			Xiaogang Huang
UNCLASSIFIED	UNCLASSIFIED	UNCLASSIFIED	UL	24	19b. TELEPHONE NUMBER (*Include area code*) 410-278-6142

Contents

List of Figures

List of Tables

Acknowledgments

The authors would like to thank Charlie Leveritt and Jeffrey Swab for providing the test figure and data that allowed this work to be accomplished.

INTENTIONALLY LEFT BLANK.

1. Introduction

The 37-mm chamber (figure 1) is a proven test bed for evaluating propellant effects in realistic ballistic environments. The U.S. Army Research Laboratory (ARL) has been tasked to evaluate the performance of ceramic nozzles in these ballistic environments. The area of the gun that appears to wear rapidly is near the origin of rifling where obturation is poor. Ceramics offer particularly good heat resistance and compressive strength and are therefore a logical choice to reduce wear in these areas and prolong life of the barrel. This is an area of concern as the high-performance propellants now in use for tactical projectiles can result in a condemned tube in as few as 175 rounds. Ceramic inserts are therefore certainly worthy of examination.

Figure 1. ARL 37-mm erosion fixture.

One of the requirements for a successful insert is its ability to withstand not only high temperatures but also high pressures simultaneously. A series of nozzles with different ceramic inserts were fabricated and placed in the 37-mm erosion fixture. The results observed in many of the samples suggested that examination of the stress states during firing was warranted and would help indicate sources of the failure. These stresses are caused by both thermal and pressure loads. A finite-element model of the 37-mm chamber was created to predict the thermal evolution and corroborate the failure modes observed.

In this analysis, thermal conductive theory and modeling methods are presented first. The finite-element thermal analysis is then performed for the full-scale gun chamber-nozzle model. A space- and time-dependent convective boundary condition is applied to the chamber and

nozzle. The peak temperatures in the ceramic nozzles and their temperature gradients are determined and discussed.

Figure 2 illustrates a quarter of a three-dimensional (3-D) finite-element model for the 37-mm gun test fixture. The chamber is fixed on a solid base, and the nozzle is placed at the front of the chamber backed up with a rupture diaphragm. A steel retainer is used to tighten the system, as shown in the figure 2. As the propellant reaches burnout , the high-pressure ruptures the diaphragm.

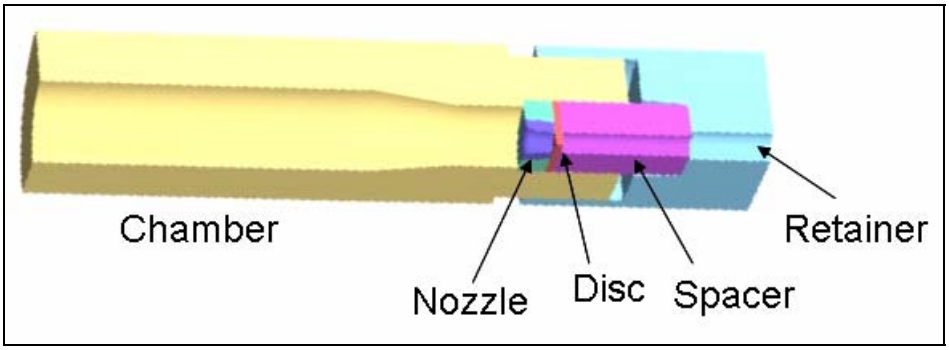

Figure 2. ARL 37-mm erosion fixture (1/4 finite-element model).

Three candidate ceramic materials are selected in this investigation. SN47 silicon nitride (Si3N4), produced by Ceradyne, Inc., is a sintered reaction bonded material that contains a small amount of yttria (Y2O3) and alumina (Al2O3) as sintering aids. The fabrication process results in a microstructure containing interlocking needle-like grains. STK4 is a SiAlON material produced by Kennametal using sintering and a post-sintering hot isostatic pressing step to produce a fully dense material. The microstructure contains elongated grains and consists of 60% alpha phase and 40% of the beta phase. ZRO2 is sintered zirconia (ZrO2) produced by CoorsTek using ceria (CeO2) to retain the meta-stability and the tetragonal phase at room temperature. This results in a transformation toughened material with high strength and toughness at room temperature.

In the simulation, the steel nozzle is modeled as the baseline. Then, the previously mentioned three ceramic nozzles are simulated and compared with the baseline.

2. Theory Background and the Chamber Gas Temperature Condition

Application of the first law of thermodynamics to the control volume yields the general conduction equation for homogeneous isotropic solid materials (*1*):

$$\frac{\partial}{\partial x}(k\frac{\partial T(x,y,z,t)}{\partial x})+\frac{\partial}{\partial y}(k\frac{\partial T(x,y,z,t)}{\partial y})+\frac{\partial}{\partial z}(k\frac{\partial T(x,y,z,t)}{\partial z})=\rho C_p\frac{\partial T(x,y,z,t)}{\partial t}. \quad (1)$$

The temperature T is defined in the domain (x, y, z) as a function of time, t. Here, ρ is the density, and C_p is the specific heat per unit mass. Isotropic thermal conductivity is represented by K. In the current case, both specific heat C_p and thermal conductivity K are temperature dependent. Since the solution of the differential equation 1 involves a number of integration constants, the completion of the formulation requires an equal number of appropriate boundary conditions in space and time to determine these constants.

2.1 Initial and Boundary Conditions

For an unsteady problem, the temperature of the continuum under consideration must be known at some instant of time. In many cases, this instant is most conveniently taken to be the beginning of the problem. If the initial condition is given by T_0, the solution of this problem returns T(r,z,t) at all points of the continuum to be specified :

$$T(r,z,t=0) = T_0 . \quad (2)$$

T_0 is taken to be the ambient temperature in our simulation.

The most commonly encountered boundary conditions are prescribed temperature, insulated wall, and convective heat transfer. These three boundary conditions can be unified as one generalized temperature boundary condition mathematically as:

$$a\frac{\partial T_s}{\partial n} = h\left(bT_s - cT\left(t\right)\right) \quad (3)$$

where $\partial/\partial n$ denotes the differentiation along the normal, T_s is the surface temperature, and $T(t)$ is the temperature at a distance far from the boundaries. The term, h, defines the effective heat transfer coefficient quantifying the convective heat flux between the surface and the environment, and the constants a, b, c are either 1 or 0 depending on the type of boundary heat transfer. If the surface temperature of the boundaries is specified to be a function of space or time, the coefficient a is zero and b and c are equal to one. When the heat transfer across the boundaries of a continuum cannot be prescribed, the constants (a, b, and c) are all equal to one. The heat flux across the surface is then proportional to the temperature difference between the boundary and the driving temperature. In the current case, the outside chamber wall is ambient temperature. The inside wall heat transfer boundary condition is convective and is discussed in the next section.

2.2 Gas Temperature and the Chamber Boundary Condition

In the past, extensive interior ballistic (IB) tests and calculations were conducted to determine the chamber temperature and internal pressure for the several propellants (*2*). Inside the chamber, the gas temperature was found to be space dependent. Especially in the nozzle area, the gas temperature has a noticeable change due to the significant geometric variation. IB

calculations coupled with a finite difference heat conduction code XBR2D v54 (REF Conroy) produced the gas-temperature profiles as well as heat-transfer coefficients as a function of time and axial location. Figure 3 shows the ex99 propellant gas-temperature profiles in the chamber. It is noted that a 200 K difference occurred for the peak temperature in axial distance from 226.1 to 238.8 mm, which is the exact nozzle position (see figure 4).

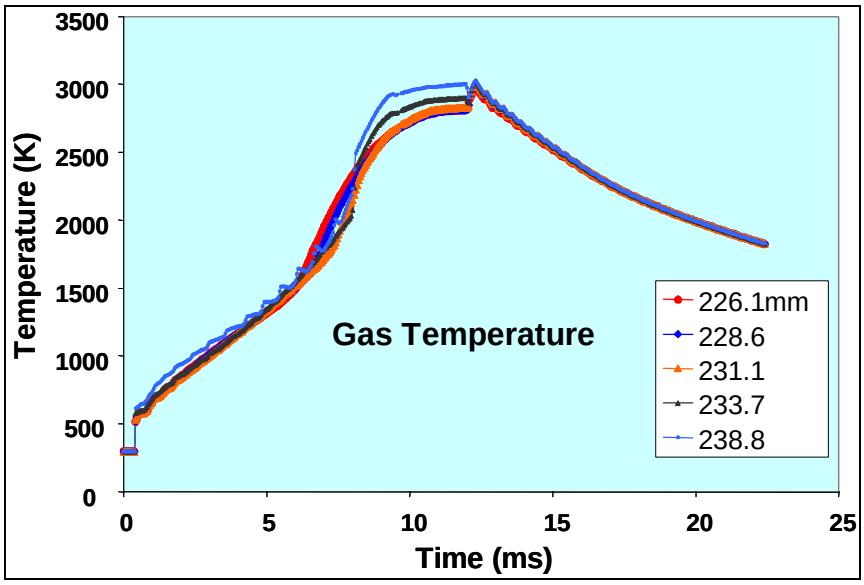

Figure 3. 37-mm erosion fixture gas-temperature profiles.

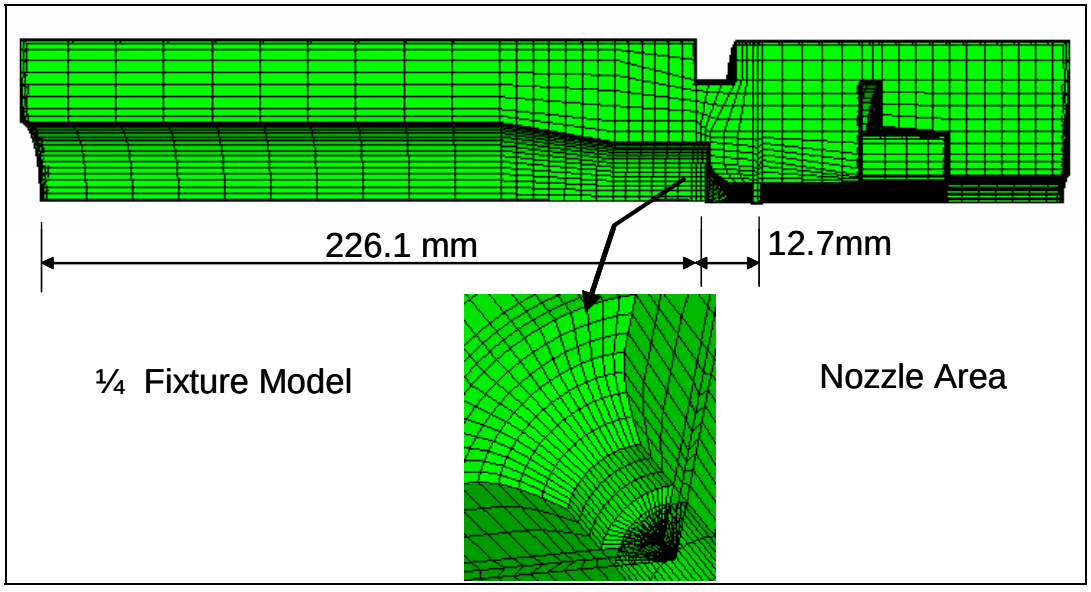

Figure 4. 37-mm experimental fixture, finite-element model.

The convective coefficient h determines the driving gas-temperature difference. In a gun system, the convective coefficient is no longer constant and behaves dynamically. In the current case, the convective coefficient is time and space dependent. According to the experimental data, the

coefficient profile was obtained using the ARL Gun Tube Heat Transfer Code (*3*) (2003 version), as shown in the figure 5. The coefficient is zero before the diaphragm ruptures at 12.5 μs. The corresponding chamber inside surface is insulated from the gas temperature. The peak values occur at 12.5 μs, after which they sharply decrease. In the nozzle area, the coefficients vary as much as 38% in the axial direction due to the flow conditions.

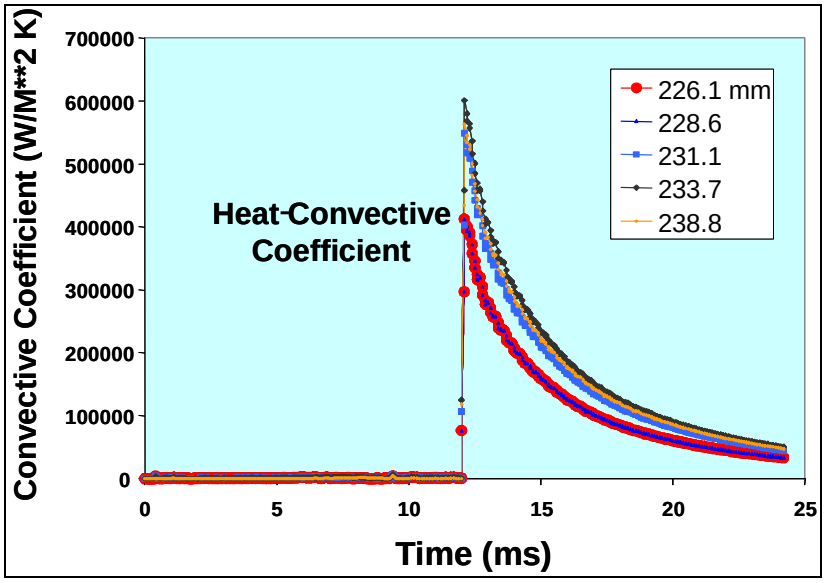

Figure 5. Time- and space-dependent, heat-convective coefficient profiles.

3. Finite-Element Approach (FEA)

When the boundaries are irregular, or when the problems involve multiple domains, there is no exact analytical solution available for the heat-conduction problem described by equation 1. Approximate integral and variational techniques are not flexible enough to handle the multidomain problem. In the past, the finite-difference method was widely used to solve such heat-conducting problems. However, for 3-D multidomain problems, the finite-difference method is extremely tedious and time consuming (*4*). In contrast, the finite-element method offers promising advantages. The finite-element code ABAQUS, developed by Hibbitt, Karlsson & Sorensen, Inc., is used to solve the heat-conducting problem formulated above (*5*).

Using ABAQUS, there is no limitation to the complexity of the geometry or the number of domains. The structure can be meshed using any suitable pre-processor code or directly using ABAQUS meshing input cards according to the user's menu, as was done for this analysis (*6*). The space- and time-dependent, gas-temperature input and convective coefficient h for the fixture can be coded by using user subroutines interfaced with the ABAQUS main code. The

formulations for the temperature and convective coefficient shown in figures 2 and 3 are externally programmed and linked into existing ABAQUS code.

In the model, shown in figure 5, the interfaces along some of the different components are fixed and the adjoining elements share common nodes at the interfaces. The total chamber length is 238.8 mm and the nozzle length is 12.7 mm. The chamber wall thickness is 25.4 mm. Three-dimensional eight-node linear brick elements were used in the model. Extra care was taken for meshing each part of the model, especially along their common edges and nozzle area. A finer mesh is used for the nozzle and its vicinity. Only one quarter of the model is used in the finite-element model simulation with the symmetric planes and the two ends having insulated boundary conditions assigned. The ABAQUS CAE software is used for post processing which includes contour plots and temperature profile curves.

3.1 Input Material Properties

In the simulation, the temperature varies from room temperature to a peak of 1200 °C. Over such a large temperature range, the material thermal conductivities and heat capacities are no longer constants. The thermal conductivities of chamber and ceramic nozzles are plotted in figure 6. It can be seen that the steel thermal conductivity changes much more dramatically with the temperature than that of the ceramic. The thermal conductivities of ceramics ZRO2 and STK4 vary little as the temperature is elevated and therefore they are treated as constants in the simulation.

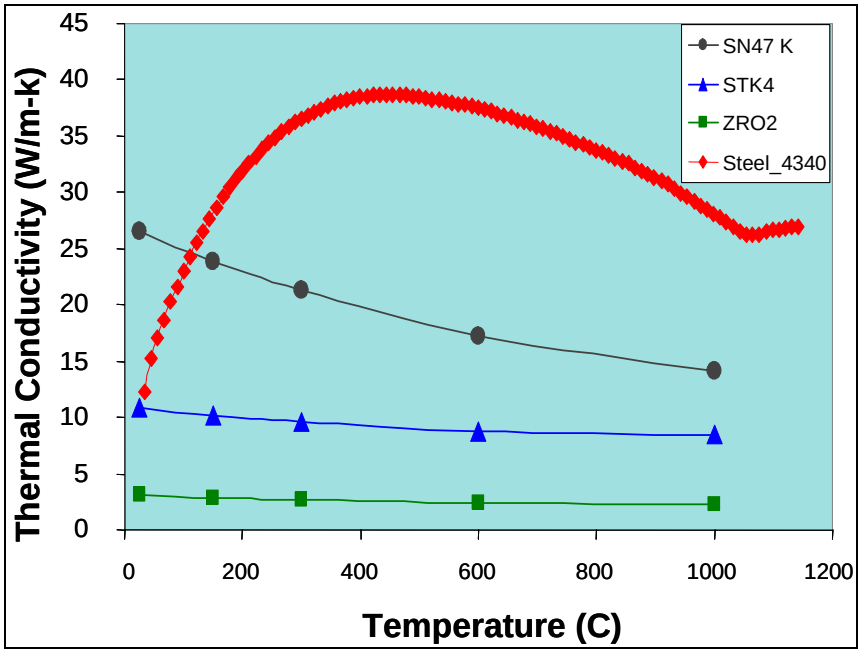

Figure 6. Thermal conductivities of steel 4340 and ceramics (*7*, *8*).

A similar situation is found for the heat capacity of these materials and is shown in figure 7. All three ceramics have thermally varying heat capacities from room temperature to 1000 °C.

The material density and coefficient of thermal expansion (CTE) for steel 4340 and ceramics are listed in table 1. It is noted that SN47 and STK4 are very close in their densities and CTE.

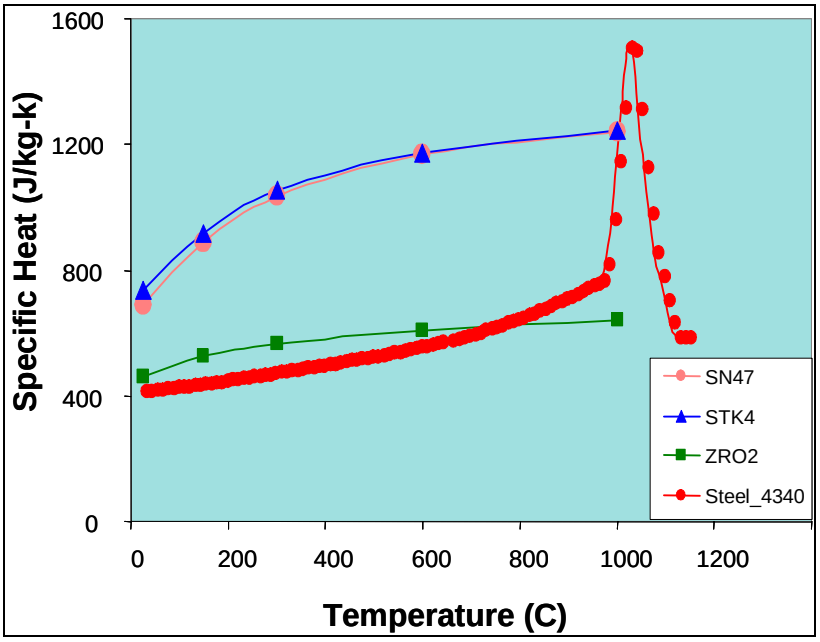

Figure 7. Heat capacities of steel 4340 and ceramics (*7*).

Table 1. Density and coefficient of thermal expansion of steel 4340 and ceramics (*7*).

Materials	Steel 4340	SN47	STK4	ZRO2
Density (kg/m^3)	7800	3200	3400	6100
CTE (10^{-6}/°C)	8.4	3.2	3.3	11.8

3.2 Model Convergence Study

The finite-element analysis simulation time step was set at a 0.1-μs increment over a total time duration of 31 μs. The number of elements used was based on the model convergence study. Figure 8 shows the model convergence result with number of elements vs. the normalized nozzle temperature. There were a total of 10 runs for the different model sizes from 4000 to 14,000 elements. A normalized nozzle-edge temperature is defined as the ratio of the nozzle-edge temperature of the model with various elements versus the temperature at the same location with 14,000 elements. Using 9000 elements, the model results converge. Further, if only the nozzle area was of interest, even fewer elements could be used by reducing number of elements in the chamber and other parts.

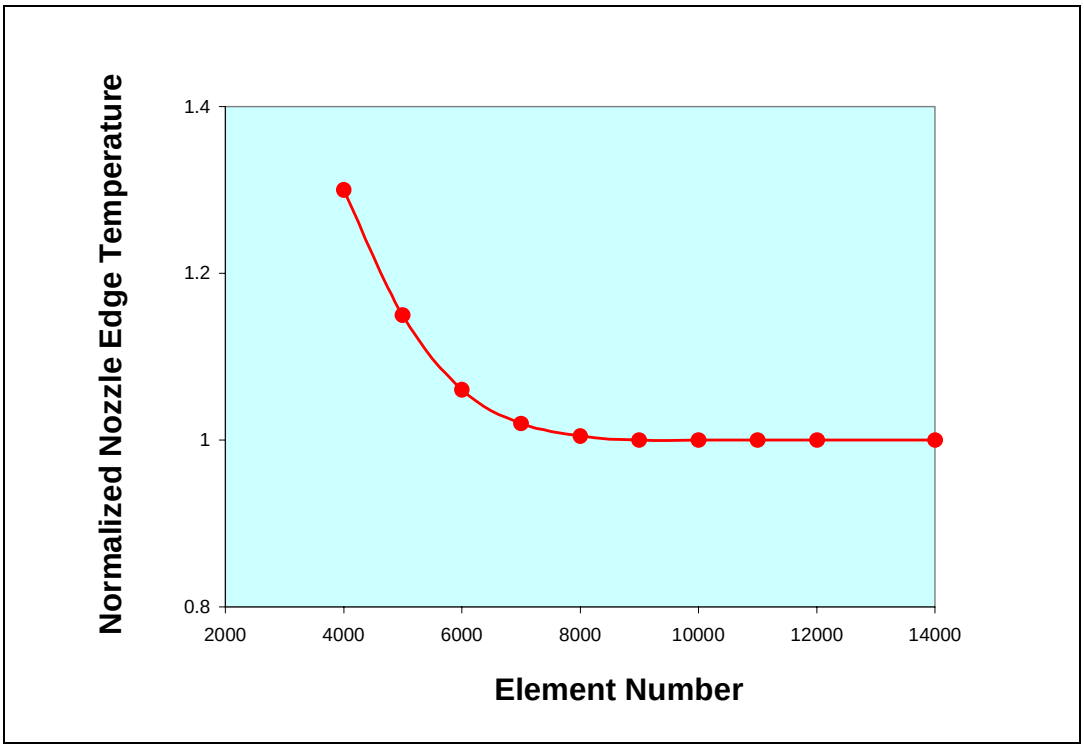

Figure 8. The variation of the nozzle temperature with the number of elements.

4. Heat Conductive Analysis of the 37-mm Gun Chamber

The simulation of the steel_4340 gun chamber with a steel_4340 nozzle is used as a baseline for comparison to nozzle ceramic materials SN47, STK4, and ZRO2. For the convenience of analysis, areas of interest in the nozzles are numbered as shown in figure 9. The nozzle entrance, throat, and top areas are denoted as number 1, 2, and 3, respectively. The gun chamber is denoted as number 4.

4.1 Temperature Contour for the Steel Chamber With Steel Nozzle

Figure 9a shows the temperature distribution in the steel_4340 nozzle and its vicinity at the IB time 17 ms, the time of peak temperature in the chamber. It is seen that the nozzle entrance (area denoted 1) has the highest temperature of 1650 °C. In the nozzle top area (area 3), the temperature is about 900 °C, while in the throat (area 2) the temperature reaches 820 °C. In the chamber region (area 4), the temperature is approximate 550 °C. The temperature gradient is captured in the simulation along the nozzle axial direction primarily because of the space-dependent gas temperature and convective coefficient.

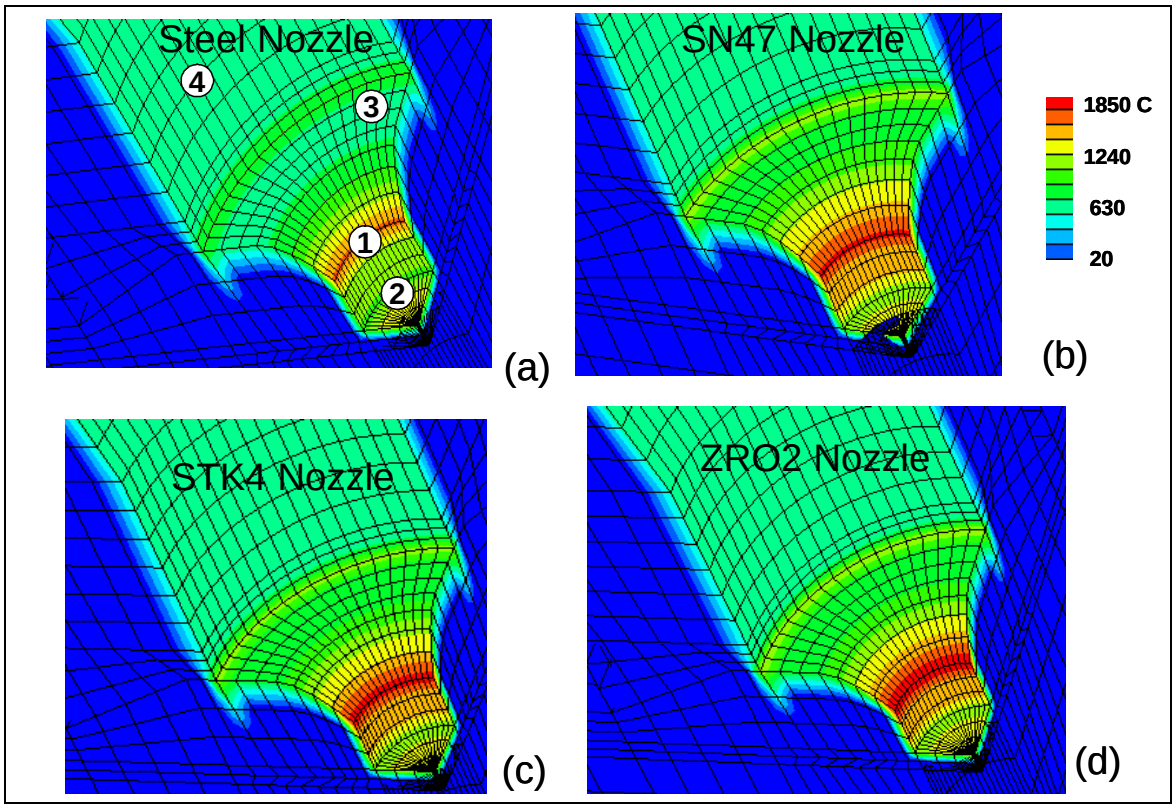

Figure 9. Temperature contours at the highest levels for the steel and ceramic nozzles.

4.2 Temperature Contours for the Steel Chamber With Ceramic Nozzles

The peak temperature distributions in the ceramic nozzles with the steel_4340 gun chamber are shown in figure 9b for SN47, figure 9c for STK4, and figure 9d for ZRO4. The thermal response not only depends on the material conductivity, but also on the material density and heat capacity (see equation 1). For the SN47 ceramic nozzle (figure 9b), the temperature in the nozzle edge can be as high as 1850 °C. In the nozzle throat and top areas, the temperatures are about 1200 and 1150 °C, respectively. The SN47 nozzle is about 250 °C higher than that computed for the steel_4340 nozzle. In the chamber area (area 4), the temperatures are all the same, regardless of the nozzle material. The temperature contour for STK4 nozzle (figure 9c) is quite close to that of SN47. The STK4 nozzle is about 30 °C lower than that of SN47 at the nozzle entrance location. By reviewing the thermal properties of these two ceramics, it is noted that they are quite similar in density, conductivity, and heat capacity (figures 6 and 7 and table 1). It therefore makes sense that they have quite similar thermal response. For the ZRO2 ceramic nozzle, the temperature is about 280 °C higher than that of the steel nozzle at the nozzle edge, throat, and top areas.

4.3 Temperature Profiles

The previous discussion is based on the peak temperature response. It is beneficial to study the temperature development throughout the ballistic cycle. Figure 10 shows the temperature

profiles as a function of time for the steel_4340 baseline and three ceramic nozzle materials in the nozzle edge and chamber areas. Corresponding to the thermal convective coefficient curve in figure 5, the temperatures remain ambient until the diaphragm ruptures at 12.5 μs. Within 4 μs, the temperatures sharply increase to their peak values. The temperatures in the nozzle edge gradually decrease until the end of in-bore time. All three ceramic nozzle temperature profiles are higher than that of the steel nozzle. The chamber temperature profiles are unaffected by the nozzle materials and are the same for each calculation.

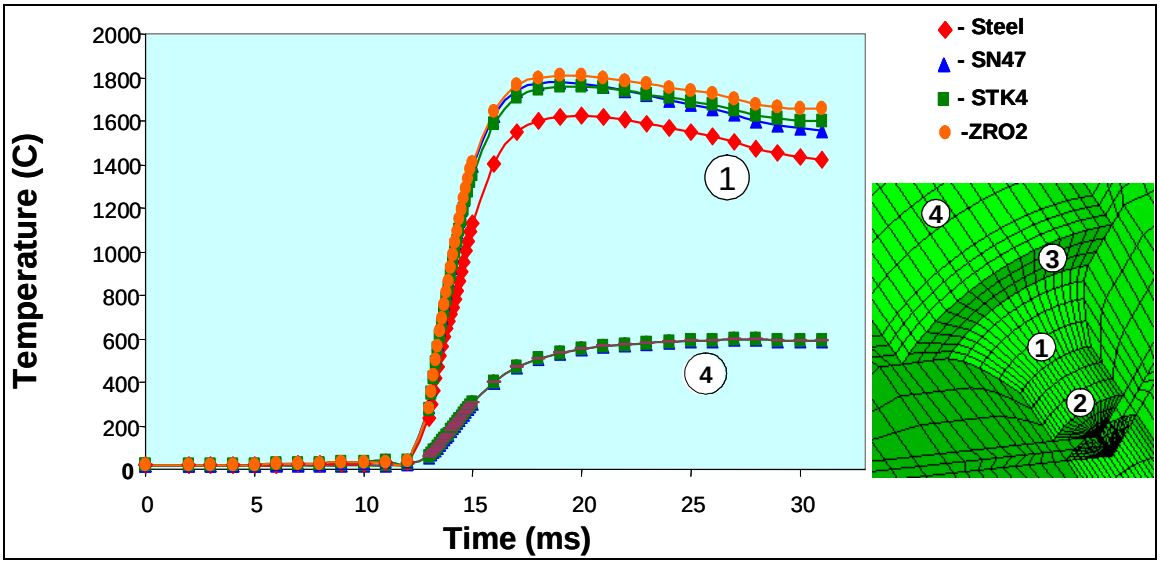

Figure 10. Thermal progressions in ceramic nozzles compared with the steel baseline in area 1.

Figures 11 and 12 show the temperature profiles in the nozzle throat and top areas (denoted 2 and 3). The temperature varies from ambient to their highest, a stable plateau near 1150 °C for the three ceramics which exhibit very similar temperature profiles while the steel nozzle temperatures are about 200 °C lower than those of the ceramics.

4.4 In-Depth Temperature Gradient

The large-temperature gradient in the nozzle wall (radial direction) could cause significant thermal stresses. In order to capture such a large temperature gradient, a very fine mesh is required. An axisymmetric ABAUQS FEA model was built, see figure 13. In this model, the four-node axisymmetric element mesh size is used with a nominal 0.01-mm dimension. The total number of elements used in the model is about 30,000. The input material properties used in the axisymmetric model are the same as those discussed in section 3.

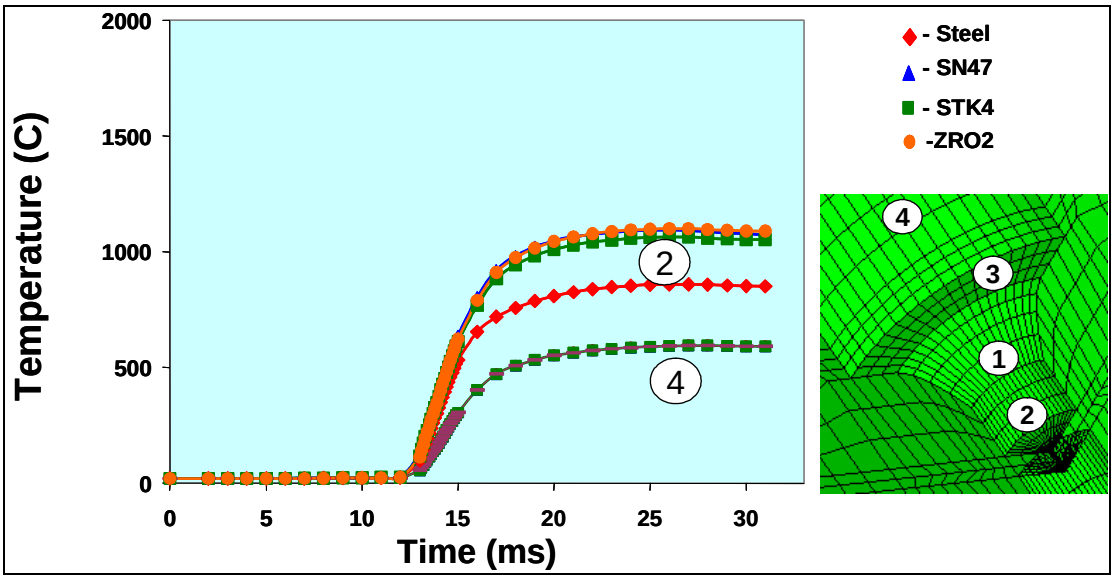

Figure 11. Thermal profiles of the ceramic nozzles compared with the steel baseline in the throat area.

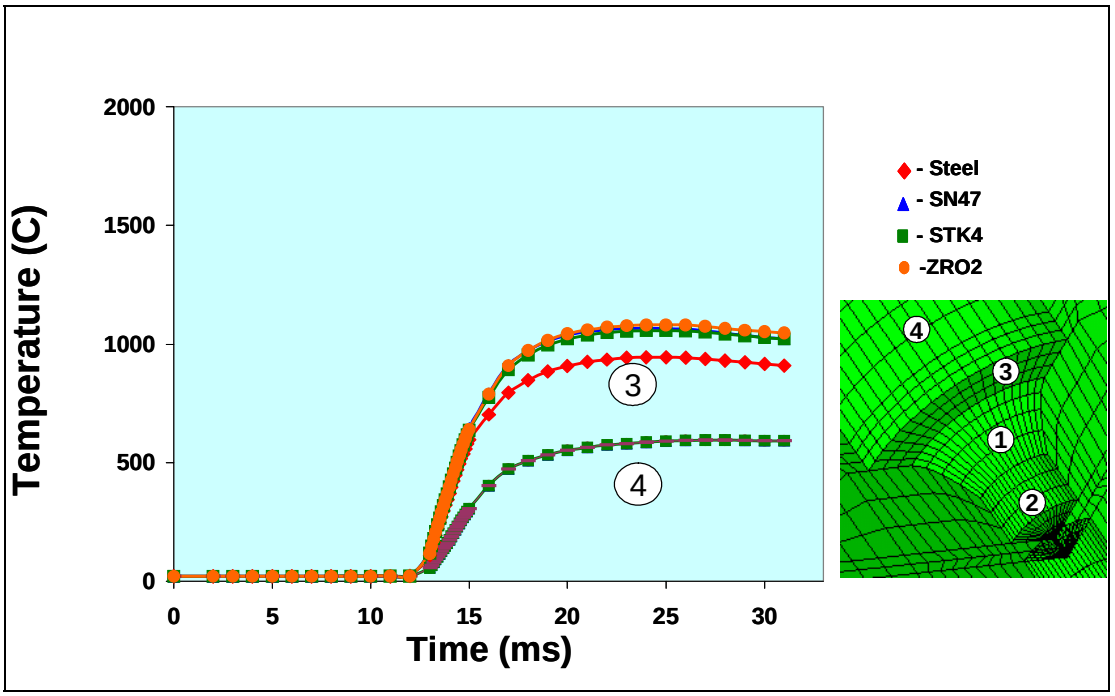

Figure 12. Thermal profiles of the ceramic nozzles compared with the steel baseline in area 3.

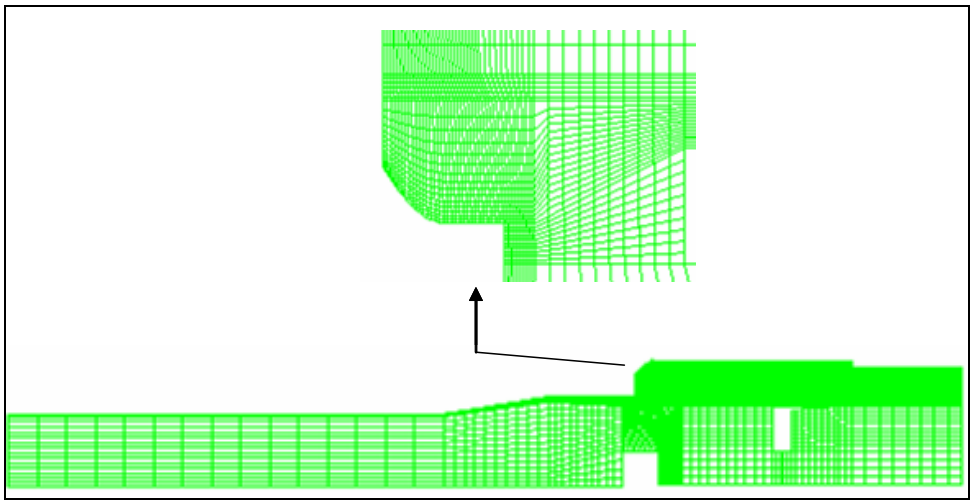

Figure 13. Axisymmetric FEA model for the nozzle test fixture.

Figure 14 shows the temperature contours for the steel and ceramic nozzles at 17 μs. It is seen that immediately in from the nozzle surfaces, the temperatures are significantly reduced in all cases. At a distance 0.2 mm under the steel nozzle surface the peak temperature is 775 °C, as shown in the figure 15. For the steel nozzle case, a 1030 °C temperature difference is noted in 0.1 mm from the surface. Similarly, the temperature gradients of ceramic nozzles for SN47, STK4, and ZRO2 are plotted in figure 16. It is expected that such large temperature gradients in depth will cause significant thermal stresses.

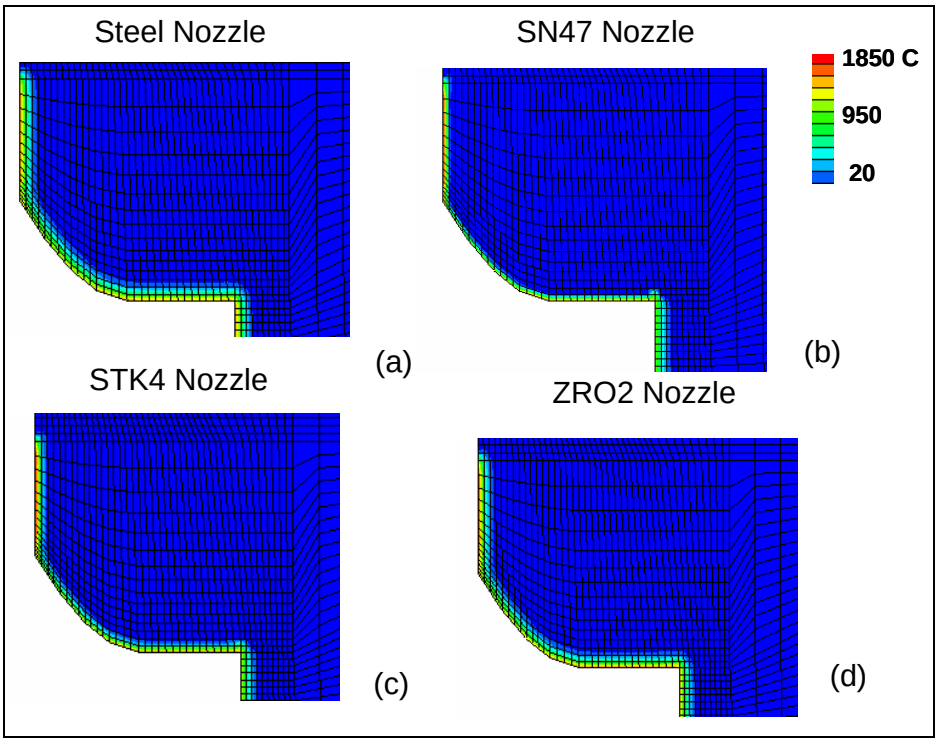

Figure 14. Axisymmetric temperature contour plots for the steel and ceramic nozzles.

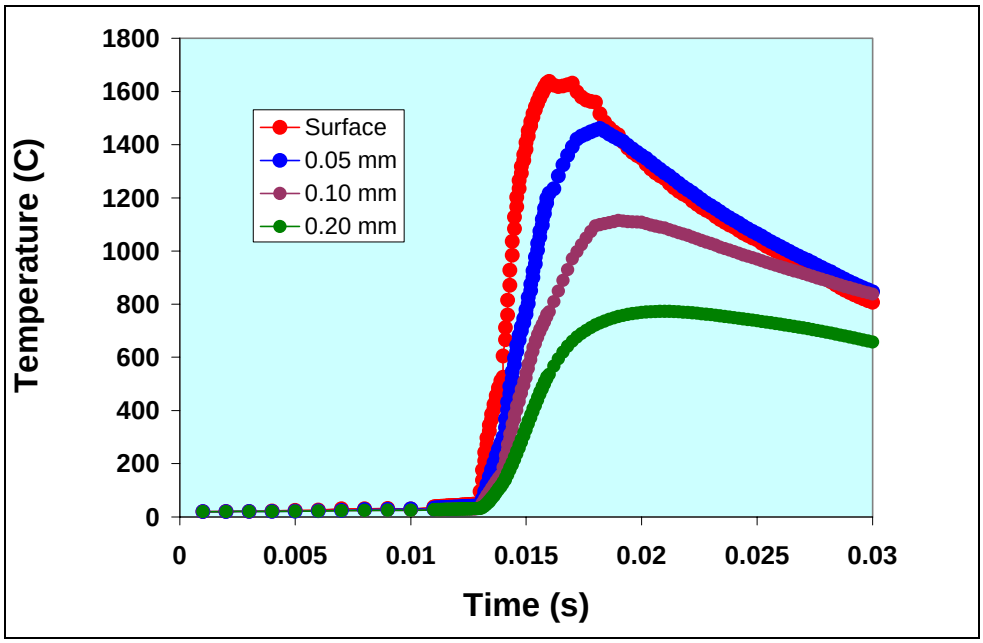

Figure 15. Temperature gradient from the surface in depth for the steel nozzle.

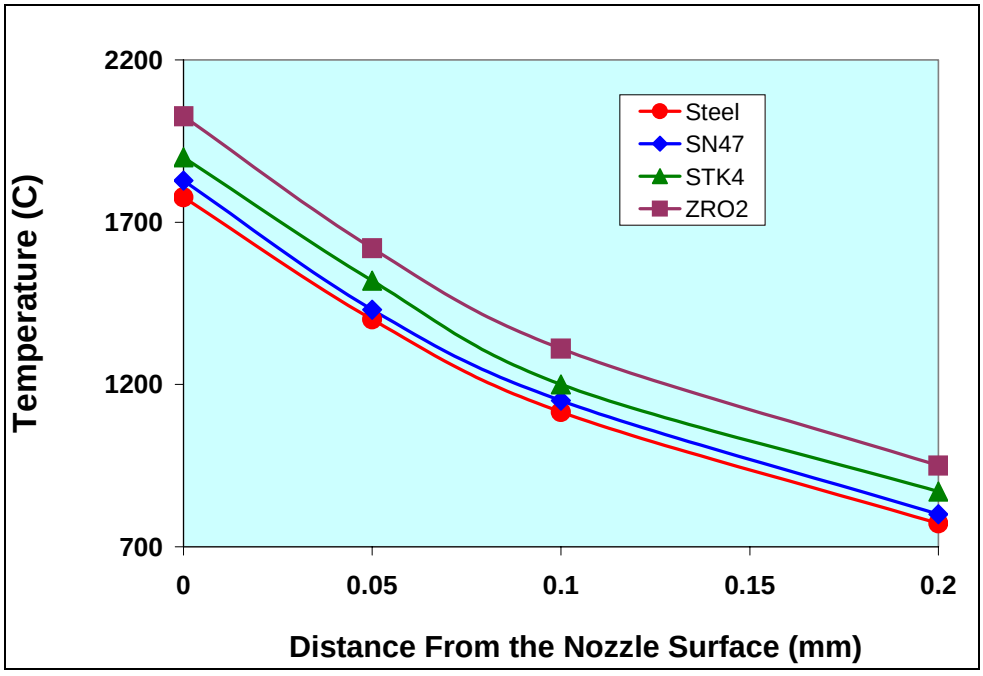

Figure 16. Radial temperature profiles under the surface for the steel and ceramic nozzles.

5. Summary

Three-dimensional FEA thermal analysis was conducted for the 37-mm erosion test fixture for a steel_4340 gun chamber with a steel and three ceramic nozzles. Previously computed data for the space-dependent, gas-temperature and convective-heat transfer coefficient was used in the analysis. Temperature-dependent heat conductivities and heat capacities were used for both the gun chamber and nozzles. The analysis shows that significant radial temperature gradients occurred in the nozzles. The nozzle entrance exhibited the highest surface temperatures. The three ceramic nozzle temperature profiles show similar trends and are approximately 200 °C higher than that of the steel nozzle, due to their relatively low thermal conductivity. The axisymmetric FEA thermal model was also built for in-wall thermal gradient analysis. Thermal profiles under the nozzle surfaces for all the materials were obtained from this analysis and are a necessary input for the future thermal stress analysis.

6. References

1. Holman, J. P. *Heat Transfer*; McGraw-Hill Book Company: New York, 1976.

2. Conroy, P.; Montgomery, J.; Lussier, L. S.; Beaupré, F.; Jones, B. *Gun Tube Wear and Erosion Final Report*; TTCP WPN/TP-4 KTA 4-26 and ARL-TR-2935; U.S. Army Research Laboratory: Aberdeen Proving Ground, MD, 2003.

3. Conroy, P. *Vented Fixture Modeling*; ARL-TR-2952; U.S. Army Research Laboratory: Aberdeen Proving Ground, MD, 2003.

4. Ames, W. F. *Numerical Methods for Partial Differential Equations*; 2nd ed.; Academic Press: New York, 1977.

5. *ABAQUS Theory Manual*; Hibbitt, Karlsson & Sorensen, Inc.: Pawtucket, RI, 1994.

6. *ABAQUS/Standard User's Manual*, vol. 1; Hibbitt, Karlsson & Sorensen, Inc.: Pawtucket, RI, 1994.

7. Swab, J. J.; Wereszczak, A. A. *Mechanical and Thermal Properties of Advanced Ceramics for Gun Barrel Applications*; ARL-TR-3417; U.S. Army Research Laboratory: Aberdeen Proving Ground, MD, 2005.

NO. OF COPIES	ORGANIZATION
1 (PDF ONLY)	DEFENSE TECHNICAL INFORMATION CTR DTIC OCA 8725 JOHN J KINGMAN RD STE 0944 FORT BELVOIR VA 22060-6218
1	US ARMY RSRCH DEV & ENGRG CMD SYSTEMS OF SYSTEMS INTEGRATION AMSRD SS T 6000 6TH ST STE 100 FORT BELVOIR VA 22060-5608
1	INST FOR ADVNCD TCHNLGY THE UNIV OF TEXAS AT AUSTIN 3925 W BRAKER LN STE 400 AUSTIN TX 78759-5316
1	DIRECTOR US ARMY RESEARCH LAB IMNE ALC IMS 2800 POWDER MILL RD ADELPHI MD 20783-1197
3	DIRECTOR US ARMY RESEARCH LAB AMSRD ARL CI OK TL 2800 POWDER MILL RD ADELPHI MD 20783-1197
3	DIRECTOR US ARMY RESEARCH LAB AMSRD ARL CS IS T 2800 POWDER MILL RD ADELPHI MD 20783-1197

ABERDEEN PROVING GROUND

1	DIR USARL AMSRD ARL CI OK TP (BLDG 4600)